Fuel 404 (2026) 136296

Contents lists available at ScienceDirect

Fuel

journal homepage: www.elsevier.com/locate/fuel

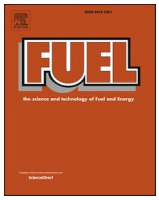

Full Length Article

Hydrocarbon generation and expulsion differences of organic matter in saline lacustrine shale: Implications for shale oil exploration and development

Miao Yu [a,b,c], Gang Gao [a,b,*], Shengnan Chen [c], Jie Li [d], Mingyu Liu [a,b], Jilun Kang [e], Xiongfei Xu [e], Wei Zhang [e]

[a] National Key Laboratory of Petroleum Resources and Engineering, Beijing 102249, China
[b] College of Geosciences, China University of Petroleum, Beijing 102249, China
[c] Department of Chemical and Petroleum Engineering, Schulich School of Engineering, University of Calgary, Calgary, AB T2N 1N4, Canada
[d] No. 8 Oil Production Plant, Changqing Oilfield Company, PetroChina, Yulin 718600, China
[e] PetroChina Tuha Oilfield Company, Hami 839009, China

ARTICLE INFO

Keywords:
Saline lacustrine shale
Hydrous pyrolysis
Organic matter
Hydrocarbon generation-expulsion-retention
Lucaogou formation
Santanghu Basin

ABSTRACT

Saline lacustrine shales are significant contributors to global oil resources, yet the mechanisms governing hydrocarbon generation, expulsion, and retention in these organic-rich fine-grained sediments remain insufficiently understood. To clarify these mechanisms among different types of organic matter, hydrous pyrolysis and pre-/post-extraction pyrolysis were conducted on representative shale samples from the Malang Sag. The experiments focused on cyanobacteria-rich shale (CRS), green algae-rich shale (GRS), and cyanobacteria and green algae mixed shale (CGMS), quantifying expelled, absorbed, and residual oil, along with hydrocarbon gases. All three shale types exhibit strong hydrocarbon generation potential, but differ significantly in expulsion efficiency and retention capacity. Within the main oil window, CRS retains the highest amount of oil, followed by CGMS and GRS. These differences are primarily controlled by variations in hydrocarbon generation timing, mineral composition, and crude oil properties. Accordingly, three conceptual models are proposed: (1) CRS—late oil generation and expulsion, narrow oil window, strong retention; (2) CGMS—early oil generation, late oil expulsion, wide oil window, moderate retention; and (3) GRS—early oil generation and expulsion, wide oil window, weak retention. Additionally, geochemical and production data reveal a maturity trend in the Malang Sag, increasing from the slope zone to the central zone. This gradient, combined with differences in organic matter composition, leads to distinct hydrocarbon generation and expulsion efficiencies, ultimately resulting in significantly higher shale oil production in the slope zone. These findings offer insights into shale oil enrichment in saline lacustrine settings and support exploration efforts in the Santanghu Basin and comparable basins globally.

1. Introduction

With the continued global growth in energy demand, particularly the increasing demand for oil and natural gas, shale oil has gradually become an important component of the global energy structure as a key unconventional oil resource [1–4]. Currently, the United States has the highest recoverable shale oil resources, followed by Russia, China, Argentina, and Libya [5]. The extraction and utilization of shale oil has provided new avenues for energy supply, especially in the context of the gradual depletion of conventional oil and gas resources. Undoubtedly, shale oil plays a significant role in filling this gap [6,7]. These developments underscore the need for improved geochemical understanding of shale oil systems, especially in relation to unconventional source rocks with diverse depositional settings. Saline lake facies shale is an important environment for shale oil accumulation. Globally, rich shale oil resources are found in saline lake facies sediments such as the Green River Formation [8,9] and Bakken Shale [10,11]. In China, significant breakthroughs have been made in the exploration of saline lake facies shale oil, with major discoveries in units such as the Fengcheng Formation in the Junggar Basin [12,13], the Lucaogou Formation

* Corresponding author.
E-mail address: gg_2819@163.com (G. Gao).

https://doi.org/10.1016/j.fuel.2025.136296
Received 1 March 2025; Received in revised form 24 June 2025; Accepted 15 July 2025
Available online 17 July 2025

[5,14], the Shahejie Formation in the Bohai Bay Basin [15], and the Qingshankou and Nenjiang Formations in the Songliao Basin [16]. These areas have revealed abundant shale oil resources, making them focal points for research and exploration in the region. However, despite the considerable progress in the study of saline lake facies shale oil, exploration and development are still in the early stages due to the complexity of the geological characteristics.

It is evident that organic-rich shales in saline lake environments store considerable oil resources. Therefore, understanding the mechanisms of oil generation, retention, and expulsion during maturation is crucial for accurately assessing the exploration potential of both conventional and unconventional oil in sedimentary basins [17]. However, the quantity and quality of hydrocarbons generated, retained, and expelled at various maturation stages of organic matter in shale remain key challenges in shale oil exploration [18]. Hydrocarbon generation and expulsion simulations, which mimic the thermal evolution of organic matter under different temperature and time conditions, are valuable tools for predicting oil and gas generation, evaluating shale oil resource potential, and examining the pyrolytic behavior of organic matter [2,19–23]. Currently, three main types of hydrocarbon generation and expulsion simulation experiments are employed: open-system, closed-system, and semi-open-system [24–28]. Of these, closed-system hydrous pyrolysis is the most widely used, as it provides valuable insights into the thermal evolution of organic matter, hydrocarbon generation kinetics, and hydrocarbon migration [22,29–32]. Moreover, hydrous pyrolysis typically offers more accurate estimates of hydrocarbon generation compared to anhydrous pyrolysis in closed systems [33,34].

The second member of Lucaogou Formation (P_2l^2) in the Santanghu Basin develops a large suite of saline lake facies shales. Previous studies have primarily focused on their geochemical characteristics [35], paleoclimate [36,37], and reservoir pore structure [38], yielding notable results. Despite this progress, characterizing the entire process of hydrocarbon generation and expulsion in saline lake facies shales remains crucial, as not all hydrocarbons generated from organic matter are recoverable [24]. Only hydrocarbons that surpass the adsorption threshold have extraction potential [39]. Thus, understanding the hydrocarbon generation and expulsion characteristics of the P_2l^2 shale is key to identifying the controlling factors for sweet spot development. However, research in this area is still in its early stages. Influenced by changes in paleoclimate conditions, saline lake basins rich in organic matter typically exhibit strong heterogeneity, reflected in both the variation in organic matter enrichment and changes in mineral composition [40]. Consequently, the ratio of expelled oil to generated oil cannot be scientifically quantified [41]. Moreover, conducting hydrocarbon generation and expulsion simulation experiments on a single organic-rich shale sample may lack scientific validity, and sample selection needs to be more representative [37,42].

The study by Yu et al. (2024a) [37] on the organic matter enrichment mechanisms of the P_2l^2 confirms that the shale primarily contains cyanobacteria and green algae as hydrocarbon-generating organic matter, with these two types of organic matter exhibiting distinct enrichment characteristics under the influence of volcanic cyclic activity. Further, Yu et al. (2024b) [43] clarified the physical properties of the hydrocarbons generated by these two types of organic matter, emphasizing that organic matter thermal evolution controls the distribution of crude oil properties in source-reservoir coupled shale oil systems. Building on these two studies, this research aims to define the hydrocarbon generation, expulsion, and retention characteristics of cyanobacteria-rich shale (CRS), green algae-rich shale (GRS), and cyanobacteria and green algae mixed shale (CGMS) in the P_2l^2. The study seeks to identify the intrinsic link between expelled and retained hydrocarbons for different organic matter types at various thermal evolution stages, providing insights for optimizing shale oil exploration and development strategies.

2. Materials and methods

The samples selected for this study are consistent with those of Yu et al. (2024b) [43] and are parallel experiments conducted on the same set of samples. In that study, CRS, GRS, and CGMS were chosen (sample details are provided in Table S1), and high-temperature, high-pressure hydrous pyrolysis was conducted using a GPM-3 pyrolysis instrument. Detailed descriptions of the experimental procedures, temperature settings, and the collection of gaseous and liquid hydrocarbon products are available in that study. During the oil washing process of the hydrous pyrolysis rock residues, we observed the attachment of a significant amounts of hydrocarbons on the surface of the residues (Fig. 1a). We believe these hydrocarbons should not be classified as expelled oil or residual oil but rather as absorbed oil (Fig. 1a-b). However, it was not possible to effectively collect this portion of hydrocarbons through soaking alone. Therefore, in this study, the rock residues from the three sets of thermal simulations were divided into two parts. Part 1 was directly crushed to a particle size of <200 μm and underwent Soxhlet extraction to obtain retained oil I. For Part 2, after crushing the rock residues, part of the samples was used for total organic carbon (TOC) content and rock pyrolysis (Rock-Eval) analysis, while the remainder underwent Soxhlet extraction to obtain chloroform asphaltene. Subsequently, the extracted rock residues were subjected to TOC and pyrolysis analysis. The pyrolysis data from Part 2 were used to calculate the yields of absorbed oil and residual oil (Fig. 2), based on the method proposed by Jarvie (2012) [2]. Detailed analytical procedures and calculation formulas are provided in the Appendix. Additionally, more than 30 Ro data points and test data from multiple wells were collected from the Tuha Oilfield Company.

3. Results

To ensure the reliability of pyrolysis parameters and accurately quantify expelled, absorbed, and residual oil yields, pre-/post-extraction pyrolysis experiments were conducted. These experiments allowed for evaluation of the residual bitumen effect on Tmax, S_1, and S_2 (Table S2), and supported a more precise assessment of liquid hydrocarbon distribution at different maturity stages. Details of the experimental procedures and results are provided in the Appendix.

CRS, GRS, and CGMS show differences in their expelled oil production stages (Fig. 3a). In the main oil window, CRS exhibits a relatively low expelled oil yield, with a production rate of about 44.66 mg/g TOC at a Ro of 0.97 %. GRS shows the highest expelled oil yield, reaching approximately 179.8 mg/g TOC at a Ro of 0.95 %. Meanwhile, CGMS experiences a slower increase in expelled oil yield, reaching about 100.95 mg/g TOC at a Ro of 0.91 %. After entering the Late oil window, CRS sees a rapid increase in expelled oil yield, peaking at 378.04 mg/g TOC at a Ro of 1.06 %. GRS and CGMS reach their peak expelled oil yields at Ro values of 1.06 % and 1.01 %, respectively, with yields of 188.56 mg/g TOC and 212.84 mg/g TOC, after which the yield gradually declines (Fig. 3a; Table S3).

Using formula (1) provided in the Appendix, the absorbed oil yields for the three samples were calculated. In the main oil window, the yield increases slowly for all three samples (Fig. 3b). After entering the Late oil window, the absorbed oil yield for GRS and CGMS slightly increases, reaching peak yields of 39.62 mg/g TOC and 41.60 mg/g TOC at Ro values of 1.06 % and 1.15 %, respectively, before gradually decreasing. In contrast, CRS experiences a more significant increase in absorbed oil yield during the Late oil window, peaking at 57.27 mg/g TOC at a Ro of 1.06 %, before gradually declining (Fig. 3b).

Residual oil yields for the three samples were calculated using formula (2) provided in the Appendix. Except for the early stages of the main oil window, where GRS exhibits a higher residual oil yield, at higher thermal evolution stages, the residual oil yield follows the pattern of CRS > CGMS > GRS (Fig. 3c). CRS, CGMS, and GRS reach their peak residual oil yields at Ro values of 0.97 %, 1.01 %, and 0.95 %,

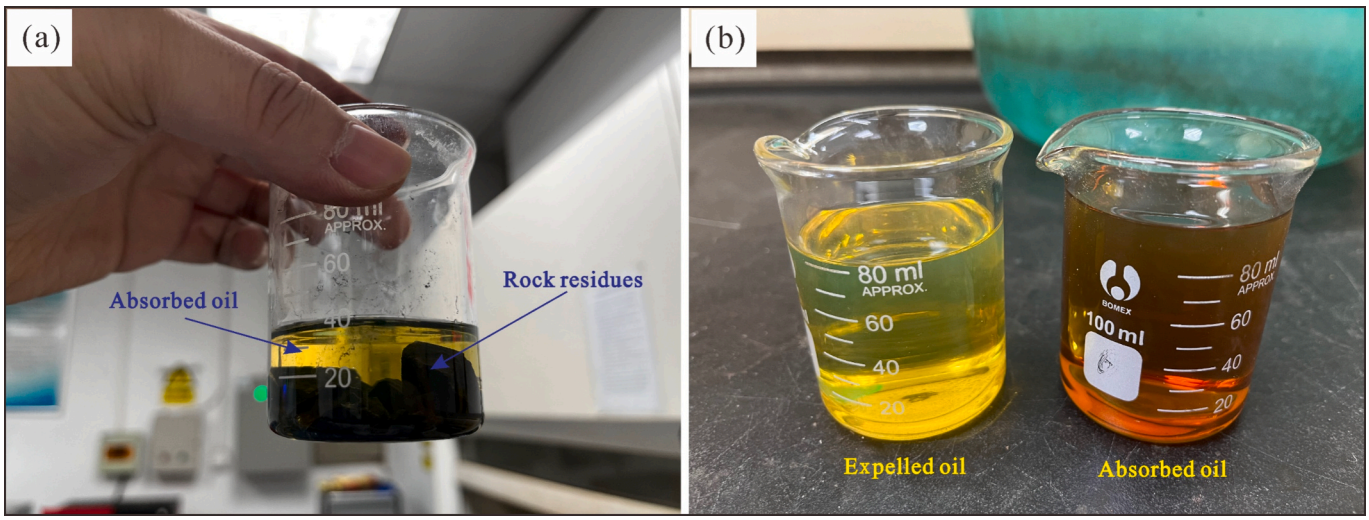

Fig. 1. Collected liquid hydrocarbons during hydrous pyrolysis showing (a) hydrocarbons adsorbed on rock residue surfaces and (b) expelled and absorbed oil separated from the pyrolysis product.

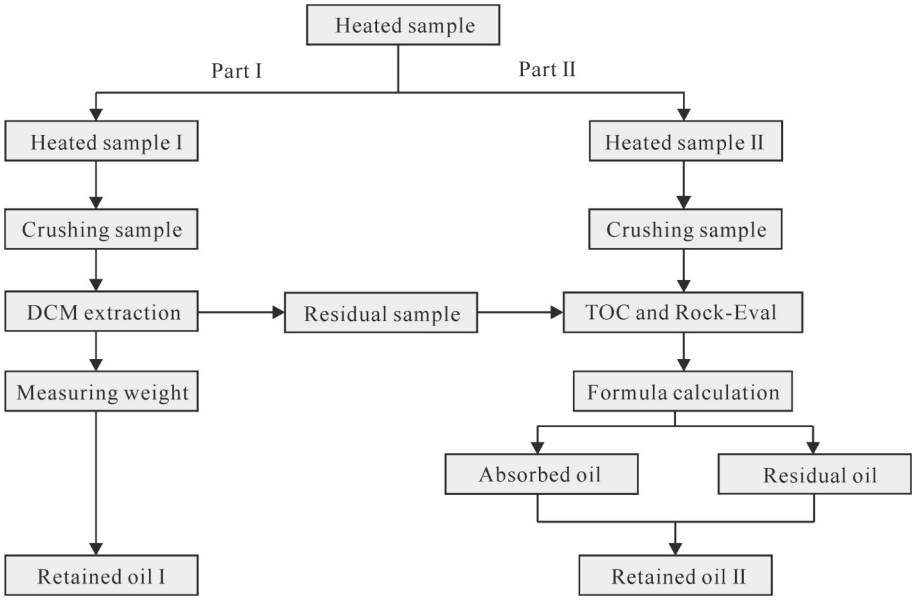

Fig. 2. Workflow diagram for the quantification of absorbed oil, residual oil, and retained oil. DCM: Dichloromethane.

respectively, with yields of 333.93 mg/g TOC, 175.97 mg/g TOC, and 138.8 mg/g TOC (Fig. 3c; Table S3).

The retained oil yields and evolutionary trends obtained using both formula (3) (Appendix) and DCM extraction methods are generally consistent (Fig. 4a–c). Therefore, the average values obtained from the two methods are used to quantify the yields (Table S3). CRS experiences a rapid increase in retained oil yield during the mid of main oil window, reaching its peak of 378.25 mg/g TOC at a Ro of 0.97 % (Fig. 4a). The retained oil yield for CGMS increases and decreases more gradually, peaking at 211.32 mg/g TOC at a Ro of 1.01 % (Fig. 4b). GRS produces retained oil primarily within the main oil window, with lower yields, peaking at 179.5 mg/g TOC at a Ro of 0.95 % (Fig. 4c). In the late oil window, GRS shows a rapid decline in retained oil yield, which is notably different from the other two samples.

The liquid hydrocarbon yield is obtained by adding the corrected retained oil and expelled oil (Table S3). The differences in liquid hydrocarbon yields among the three sample groups primarily reflect variations in the width of the oil window, the Ro at the peak of oil generation, and the amount of oil generated at the peak (Fig. 5a; Table S3). Overall, GRS and CGMS generate a significant quantity of liquid hydrocarbons at lower organic matter maturities, peaking at Ro values of 0.95 % and 1.01 %, respectively, with peak liquid hydrocarbon yields of 359.3 mg/g TOC and 424.16 mg/g TOC. The yield curves for these two samples change relatively smoothly, with substantial liquid hydrocarbon generation throughout the entire oil generation phase (Fig. 5a). In contrast, CRS experiences a relatively late peak in hydrocarbon generation. After the late main oil window, the liquid hydrocarbon yield increases rapidly, reaching its peak of about 586.67 mg/g TOC at a Ro of 1.06 % (Fig. 5a).

The trends in hydrocarbon gas yield for the three samples are relatively consistent (Fig. 5b; Table S3). During the main oil window, the yields are relatively low, but in the late oil window, the hydrocarbon gas yield rises rapidly. At the highest maturity level in this simulation, GRS, CRS, and CGMS have yields of 342.39 mg/g TOC, 350.9 mg/g TOC, and 339.37 mg/g TOC, respectively (Fig. 5b).

Hydrocarbon expulsion efficiency (HEE), referring to the efficiency

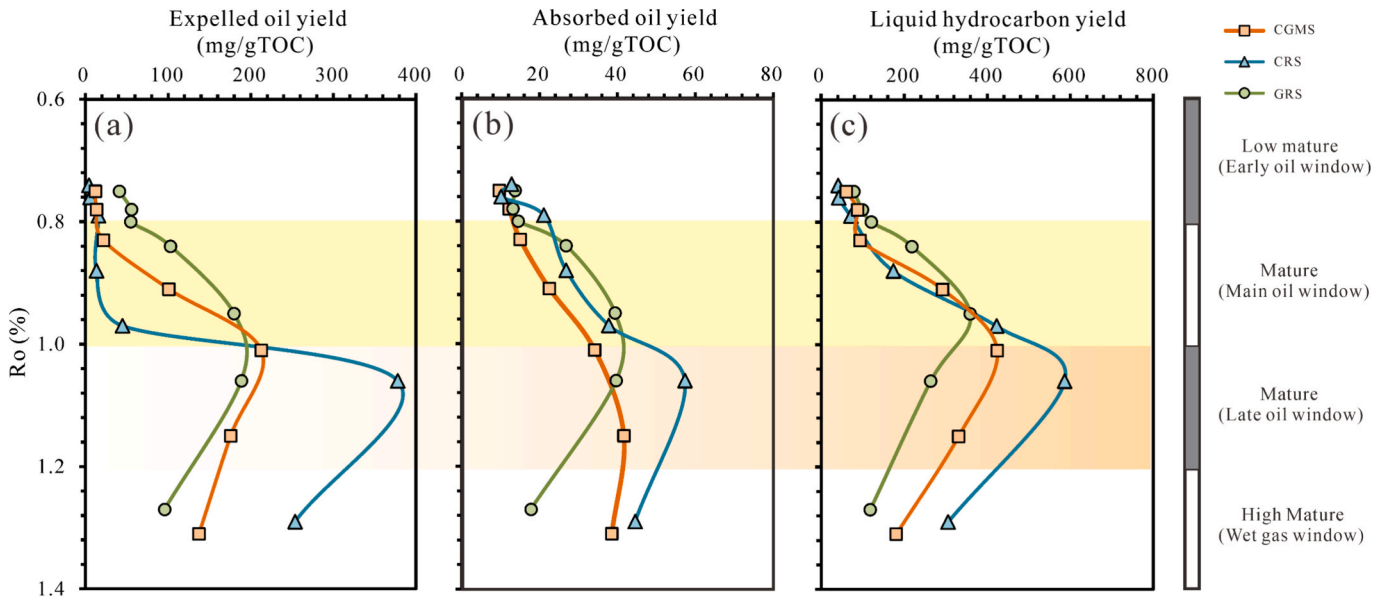

Fig. 3. Yields of expelled oil (a), absorbed oil (b), and residual oil (c) during pyrolysis of CRS, CGMS, and GRS samples; CRS: cyanobacteria-rich shale; CGMS: cyanobacteria and green algae mixed shale; GRS: green algae-rich shale. (For interpretation of the references to colour in this figure legend, the reader is referred to the web version of this article.)

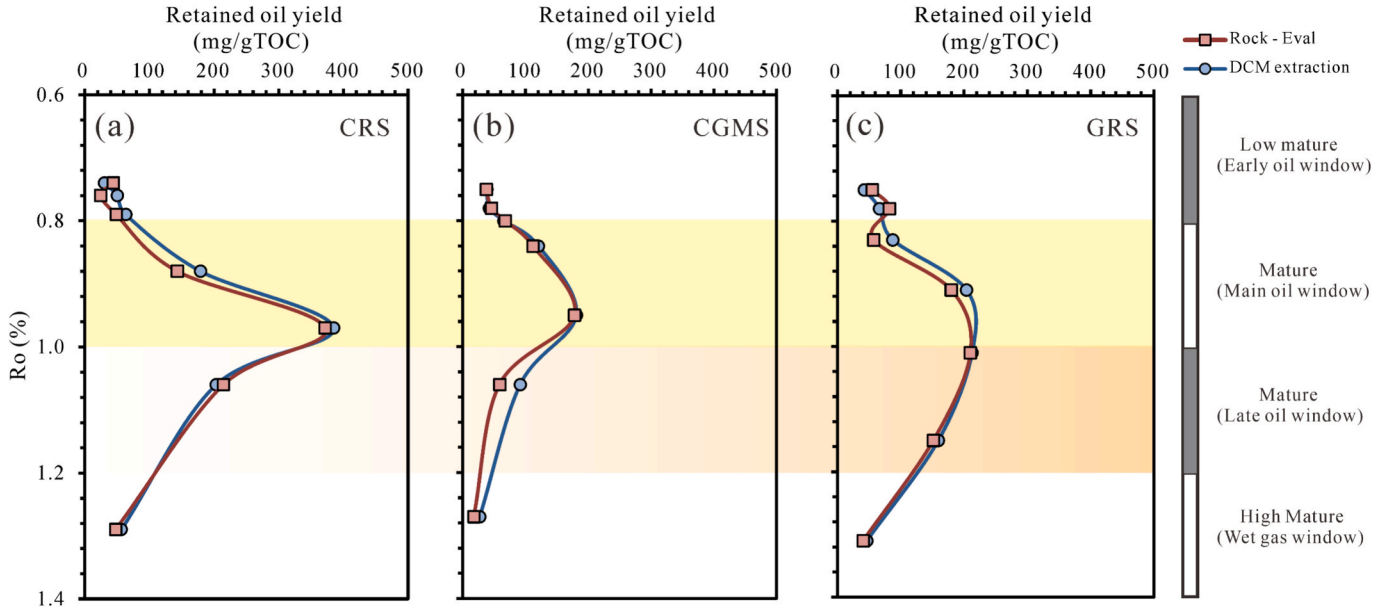

Fig. 4. Retained oil yield during the pyrolysis process of CRS (a), CGMS (b), and GRS (c); CRS: cyanobacteria-rich shale; CGMS: cyanobacteria and green algae mixed shale; GRS: green algae-rich shale. (For interpretation of the references to colour in this figure legend, the reader is referred to the web version of this article.)

of primary hydrocarbon migration, is one of the key components in shale oil resource evaluation [24,44], with researchers defining and calculating it differently based on their methods. The specific calculation method used in this study is provided in the Appendix. The HEE of GRS gradually increases with higher maturity, with a slightly slower growth rate in the main oil window, which is related to the higher rate of retained oil growth during this stage (Fig. 6a). This trend is similar with the experimental results of Ma et al. (2020) [45]. However, the HEE of CRS is significantly suppressed in the main oil window, with a value of only 23.15 % at a Ro of 0.97 % (Fig. 6b; Table S3), as a considerable quantity of hydrocarbons are retained and unable to be expelled. In addition, compared to GRS, the HEE growth of CGMS is also noticeably slower (Fig. 6c), with more than half of the hydrocarbons retained (Table S3), and the HEE is consequently somewhat suppressed.

4. Discussion

4.1. Factors influencing hydrocarbon expulsion efficiency

The factors influencing HEE are complex, with different researchers focusing on different aspects [24,39,46,47]. Generally, the amount of hydrocarbon generation directly determines the scale of oil and gas production, influencing both the accumulation of oil and gas in the source rock and the expulsion process, with higher hydrocarbon generation typically leading to higher HEE [48]. The rate of hydrocarbon generation is directly related to the speed at which organic matter

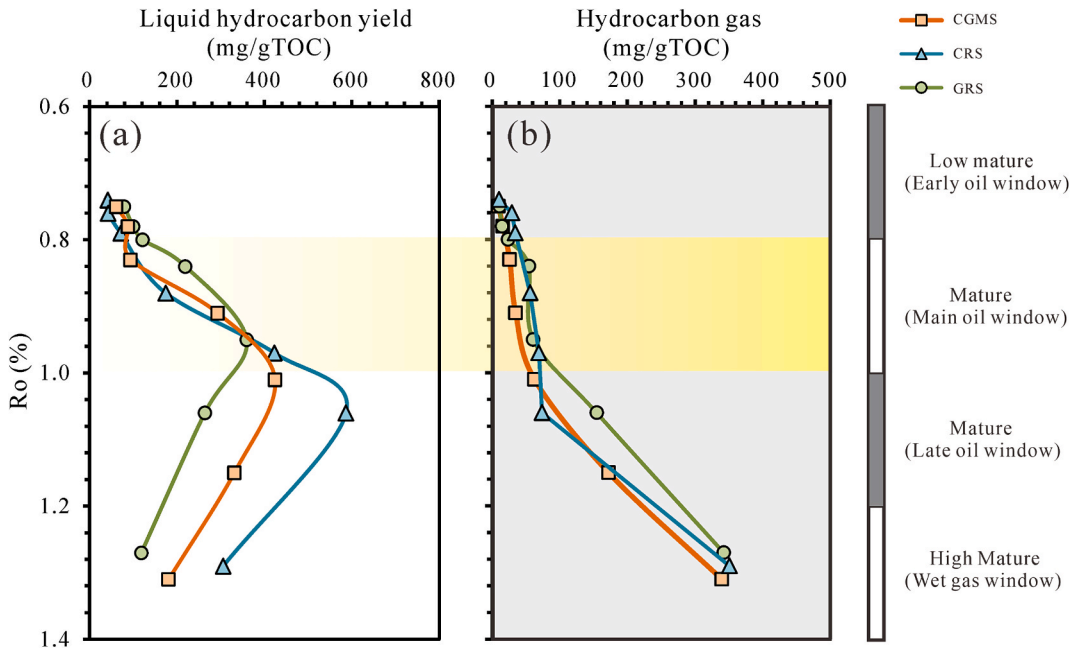

Fig. 5. Liquid hydrocarbon (a) and hydrocarbon gas (b) yields during pyrolysis of CRS, CGMS, and GRS; CRS: cyanobacteria-rich shale; CGMS: cyanobacteria and green algae mixed shale; GRS: green algae-rich shale. (For interpretation of the references to colour in this figure legend, the reader is referred to the web version of this article.)

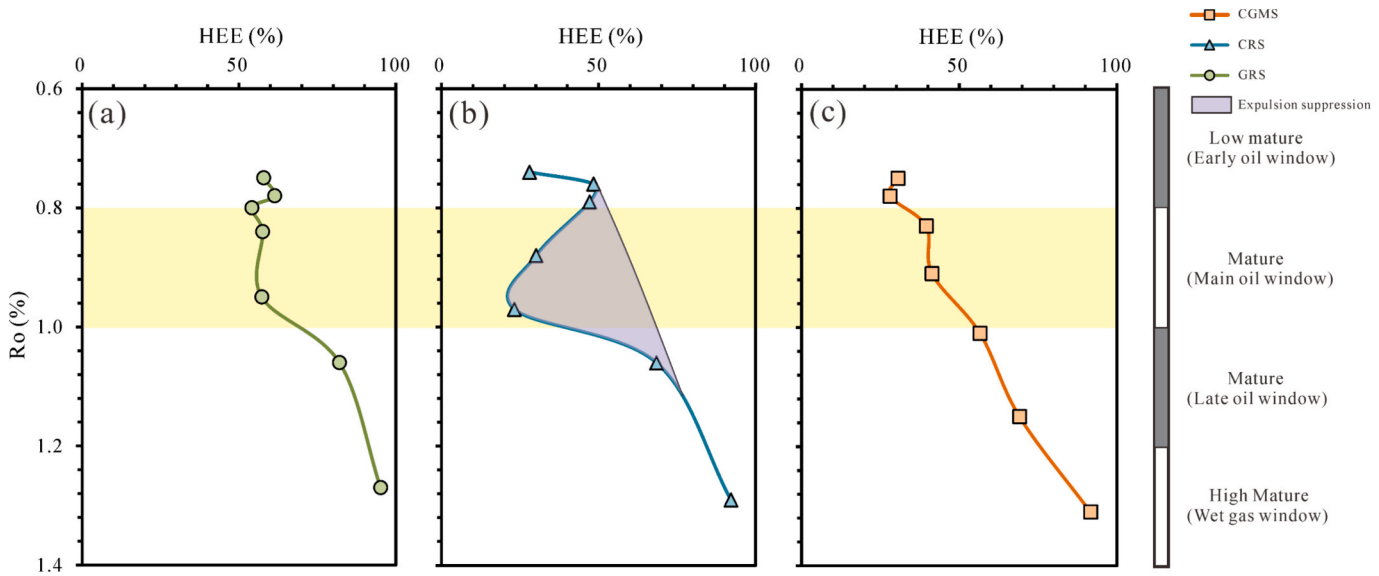

Fig. 6. Changes in HEE during pyrolysis of GRS (a), CRS (b), and CGMS (c); GRS: green algae-rich shale; CRS: cyanobacteria-rich shale; CGMS: cyanobacteria and green algae mixed shale. (For interpretation of the references to colour in this figure legend, the reader is referred to the web version of this article.)

undergoes pyrolysis to produce oil and gas, which in turn determines the volume and pressure accumulation of oil and gas in the source rock [39]. During the rapid hydrocarbon generation phase, the expanding volume of generated oil and gas creates higher pore pressure, and the accumulation of this pressure helps drive the migration of oil and gas, thus enhancing the expulsion capacity [49,50].

In the main oil window, the differences in hydrocarbon gas yield among the three samples are minimal, generally less than 70 mg/g TOC. Therefore, HEE is primarily influenced by liquid hydrocarbon yield (Fig. 6; Table S3). The liquid hydrocarbon yields of the three samples increase rapidly in the main oil window, but the generation rate follows the pattern of GRS > CGMS > CRS (Fig. 5a; Table S3). However, compared to the other two samples, CRS produces a significant amount of retained oil during this phase (Fig. 4a), and although the expelled oil yield slightly increases, the increase is minimal, directly leading to a severe suppression of HEE for CRS during this stage.

Generally, as organic matter maturity increases, large molecules in hydrocarbons gradually crack into smaller molecules, with the light components in crude oil increasing and the expulsion rate of expelled oil typically exceeding that of retained oil, leading to a gradual increase in shale HEE [51,52]. However, in shale formations with poorer reservoir properties, the density and viscosity of crude oil directly control fluid mobility, which in turn affects shale HEE [53]. Light crude oil typically has a higher saturated hydrocarbon content, lower viscosity, and better flowability, facilitating the migration of oil and gas from the source rock. In contrast, heavy crude oil, rich in asphaltenes and resins, has a high

viscosity and strong adsorption properties, making it less mobile and more likely to be retained in organic matter pores, thus reducing HEE [54]. Additionally, the increase in polar components in crude oil enhances the rock's affinity for oil, causing the crude oil to be more easily retained on the rock surface, which reduces HEE [24,39]. Therefore, the continuous decrease in HEE for CRS in the main oil window may be related to changes in the composition of the crude oil.

The analytical experimental results of these three samples by Yu et al. (2024b) [43] show that, as organic matter maturity increases, liquid hydrocarbons first become heavier and then lighter. Specifically, the heavy component content (aromatic hydrocarbons + resins + asphaltenes) in the liquid hydrocarbon composition first increases and then decreases. At the peak of oil generation, the physical properties of the liquid hydrocarbons are at their worst. This characteristic has been confirmed by studies from Ruble et al. (2003) [9], Gao et al. (2023) [55], Yu et al. (2023) [56], and Liu et al. (2024) [57]. For CRS, the main suppression range is between Ro values of 0.76 % and 1.06 %, as its thermal evolution during this stage is close to the oil generation peak. Therefore, the poor physical properties of crude oil are an important factor contributing to the generally low HEE during this stage. Additionally, the heavy component content in CRS is generally higher than in the other two samples [43], resulting in the most significant suppression. For shale oil, the amount of retained hydrocarbons determines the exploration value of the shale [52]. However, a higher content of retained hydrocarbons does not necessarily indicate greater shale oil exploration potential. A large amount of high-molecular-weight liquid hydrocarbons trapped in shale is also difficult to produce [18]. Only hydrocarbons with a high content of small molecules in free form have production potential [58]. Therefore, although CRS has a higher content of retained hydrocarbons in the main oil window, its production potential is limited due to the poor properties of its hydrocarbons. As a result, in shale oil exploration, factors such as the density, viscosity, and other properties of the hydrocarbons, in addition to their quantity, should also be considered [59].

Moreover, it should be noted that the mineral composition of rocks indirectly affects HEE by influencing the rock's physical properties and the migration path of oil and gas [60,61]. Yu et al. (2024a) [37] suggest that green algae are often associated with carbonate minerals, with the dominant lithology being tuffaceous dolomite, while cyanobacteria are associated with feldspar-rich minerals, with the predominant lithology being tuff and dolomitic tuff. In contrast, the lithology of green algae and cyanobacteria mixed development is primarily transitional, consisting of

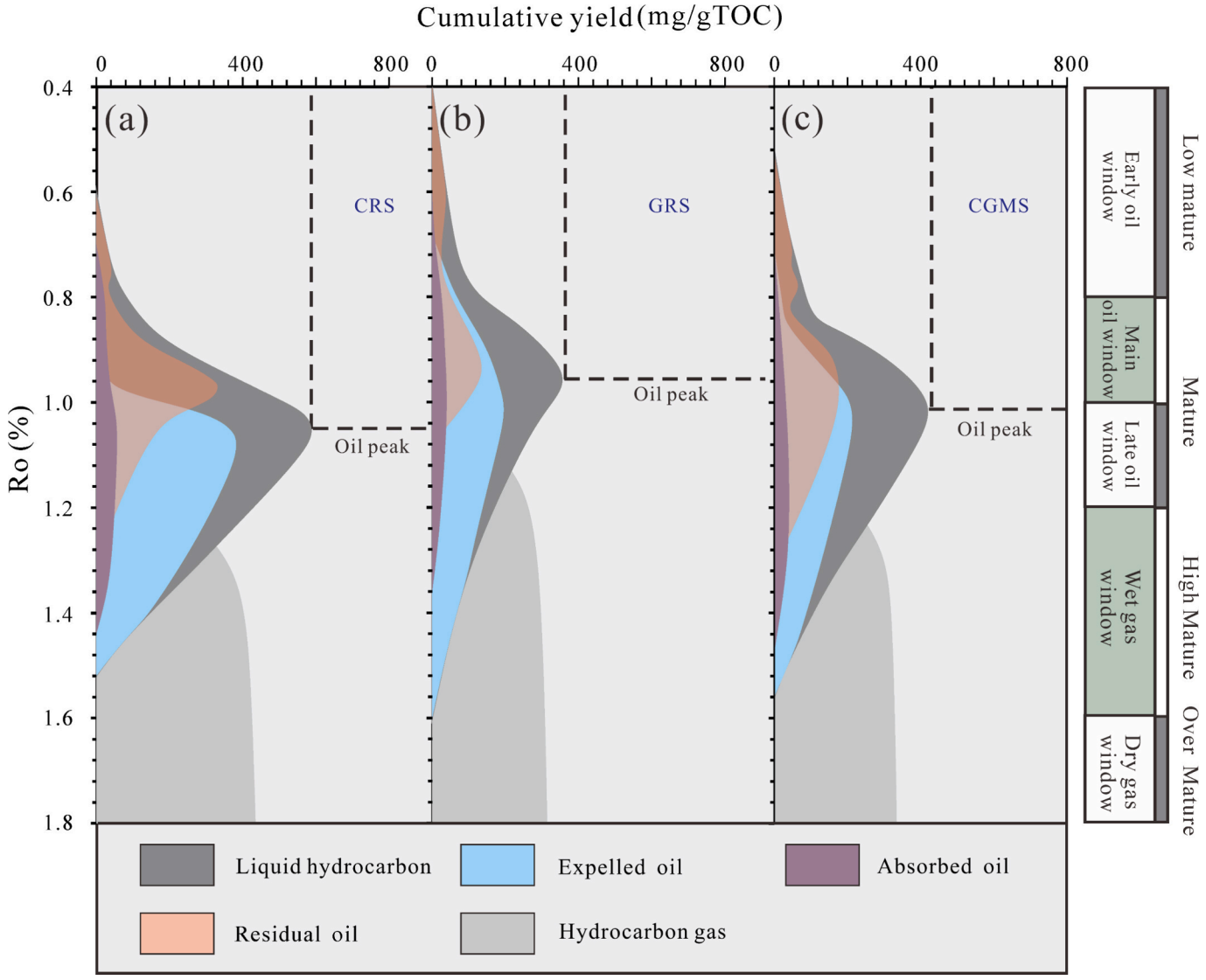

Fig. 7. Hydrocarbon generation and expulsion models of CRS (a), GRS (b), and CGMS (c); CRS: cyanobacteria-rich shale; GRS: green algae-rich shale; CGMS: cyanobacteria and green algae mixed shale. (For interpretation of the references to colour in this figure legend, the reader is referred to the web version of this article.)

dolomitic tuff and tuffaceous dolomite. Carbonate minerals like dolomite have high solubility, allowing them to form secondary pores through dissolution, which are often larger and, to some extent, enhance the rock permeability, providing more pathways for fluid flow [62–67]. In comparison, the pores in feldspar-rich shale are typically smaller, relying mainly on microfractures for hydrocarbon expulsion, and the permeability is generally poorer [38,68]. Therefore, the severe suppression of HEE in CRS within the main oil window may be related to the poor pore structure of feldspar-rich shale, while the higher proportion of dolomite in GRS and CGMS allows for stronger dissolution during organic matter hydrocarbon generation, leading to a weaker suppression of HEE.

4.2. Hydrocarbon expulsion mechanism and HGE models

Using expelled oil, absorbed oil, residual oil, liquid hydrocarbon yield, and hydrocarbon gas yield, the CRS—late oil generation and expulsion, narrow oil window, strong retention model (Fig. 7a), GRS—early oil generation and expulsion, wide oil window, weak retention model (Fig. 7b), and CGMS—early oil generation, late oil expulsion, wide oil window, moderate retention model (Fig. 7c) were established. These three distinct models reflect their respective

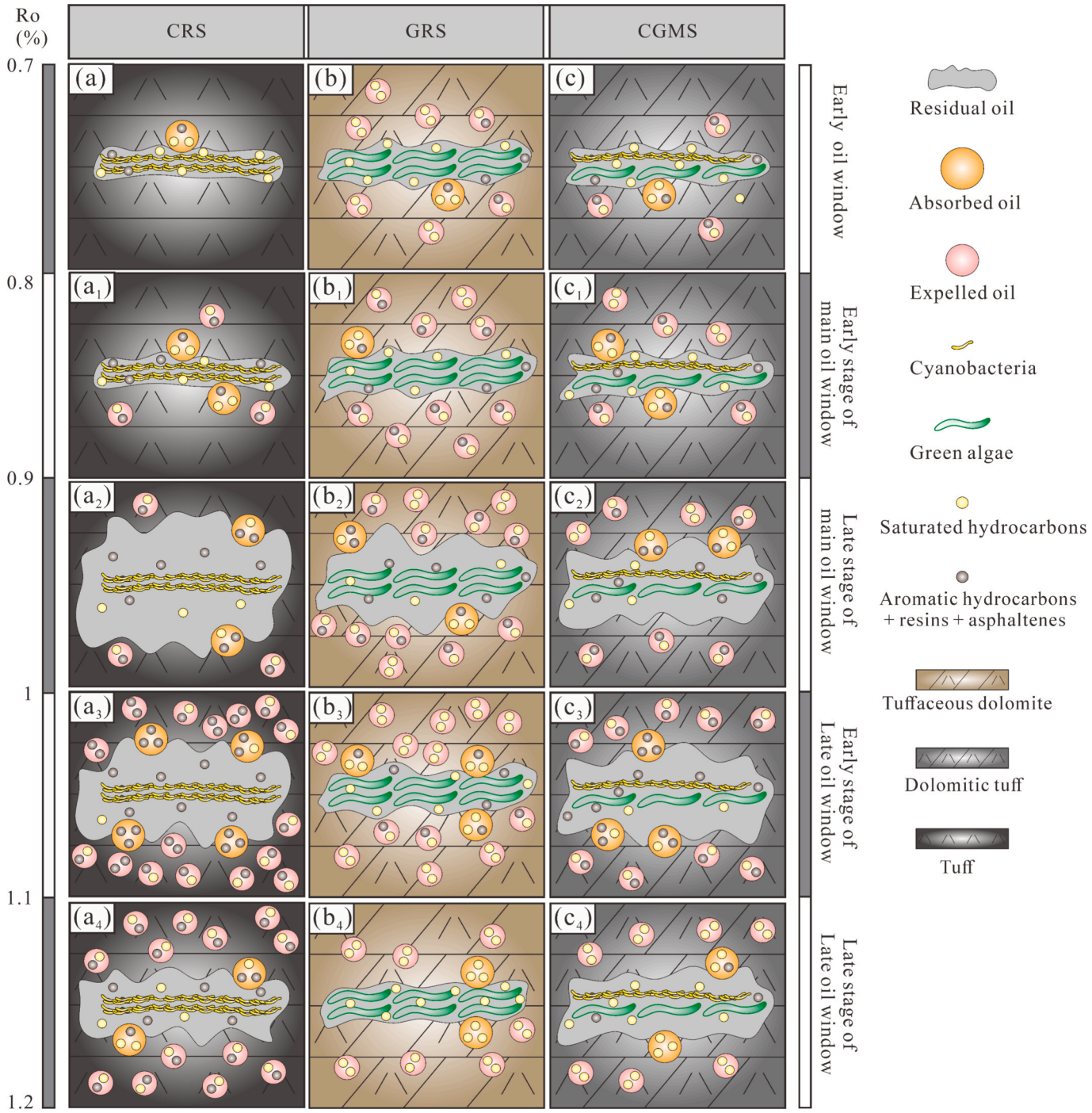

Fig. 8. Hydrocarbon generation, expulsion, and retention mechanisms during pyrolysis of CRS (a–a_4), GRS (b–b_4), and CGMS (c–c_4); CRS: cyanobacteria-rich shale; GRS: green algae-rich shale; CGMS: cyanobacteria and green algae mixed shale. (For interpretation of the references to colour in this figure legend, the reader is referred to the web version of this article.)

hydrocarbon generation, expulsion, and retention mechanisms, primarily manifested in the following stages:

In the Early oil window, hydrocarbons formed by kerogen transformation in CRS primarily exist as retained oil (Fig. 8a), as the overpressure generated during the transformation is insufficient to create expulsion pathways, while adsorption and nanopore constraints hinder hydrocarbon migration [39,69,70]. However, GRS and CGMS contain more expelled oil (Fig. 8b and c), which is related to their ability to generate a larger amount of light oil at lower maturities [43].

In the main oil window, residual oil gradually transforms into absorbed oil and expelled oil, with fluid pressure and pore volume steadily increasing, which leads to the formation of interconnected pores and microfractures, thereby causing the expelled oil yield to gradually increase [71–75]. However, there are differences in the rate of increase in expelled oil among the three samples. In the early stage of the main oil window, GRS and CGMS begin to expel a considerable quantity of hydrocarbons (Fig. 8b1 and c1), while CRS has a lower expelled oil yield (Fig. 8a1). By the late stage of the main oil window, although the heavy component content in the generated hydrocarbons of GRS and CGMS continues to increase, the expelled oil yield continues to rise (Fig. 8b2 and c2), which is associated with their relatively weak suppression of HEE. In contrast, the expelled oil yield of CRS shows little change (Fig. 8a2), as the hydrocarbons generated in CRS during this stage are primarily in the form of residual oil, reaching the peak yield of residual oil, reflecting the stronger suppression of HEE during this stage.

In the late oil window, GRS contains almost no residual oil (Fig. 8b3 and b4), and hydrocarbons continue to expel, accompanied by the conversion of liquid hydrocarbons to gaseous hydrocarbons, causing the expelled oil yield to gradually decrease. However, CRS exhibits a unique evolution during this stage, characterized by a significant increase in expelled oil yield in the early stage of the late oil window, while the residual oil yield does not decrease significantly (Fig. 8a3). During this phase, both the retained oil and expelled oil in CRS have a very high heavy component content. This contrasts with previous understanding, which generally suggests that, during oil expulsion, heavier components are retained in the source rock rather than lighter components [24,46,76]. This phenomenon suggests that when the hydrocarbons generated by kerogen exceed the critical oil saturation or absorption threshold of the rock [24,25,41], heavier hydrocarbons may also be expelled. In other words, the timing of shale hydrocarbon expulsion is primarily related to the ratio of generated hydrocarbons to kerogen, where a low ratio results in asphaltenes remaining dissolved in kerogen as retained oil, while a high hydrocarbon content and kerogen saturation lead to a gradual increase in expelled oil yield [77,78]. By the late stage of the late oil window, the residual oil yield of CRS gradually decreases (Fig. 8a4), accompanied by the generation of hydrocarbon gases, while the expelled oil yield continues to decline, though the heavy component content remains high. In contrast, CGMS shows a slight

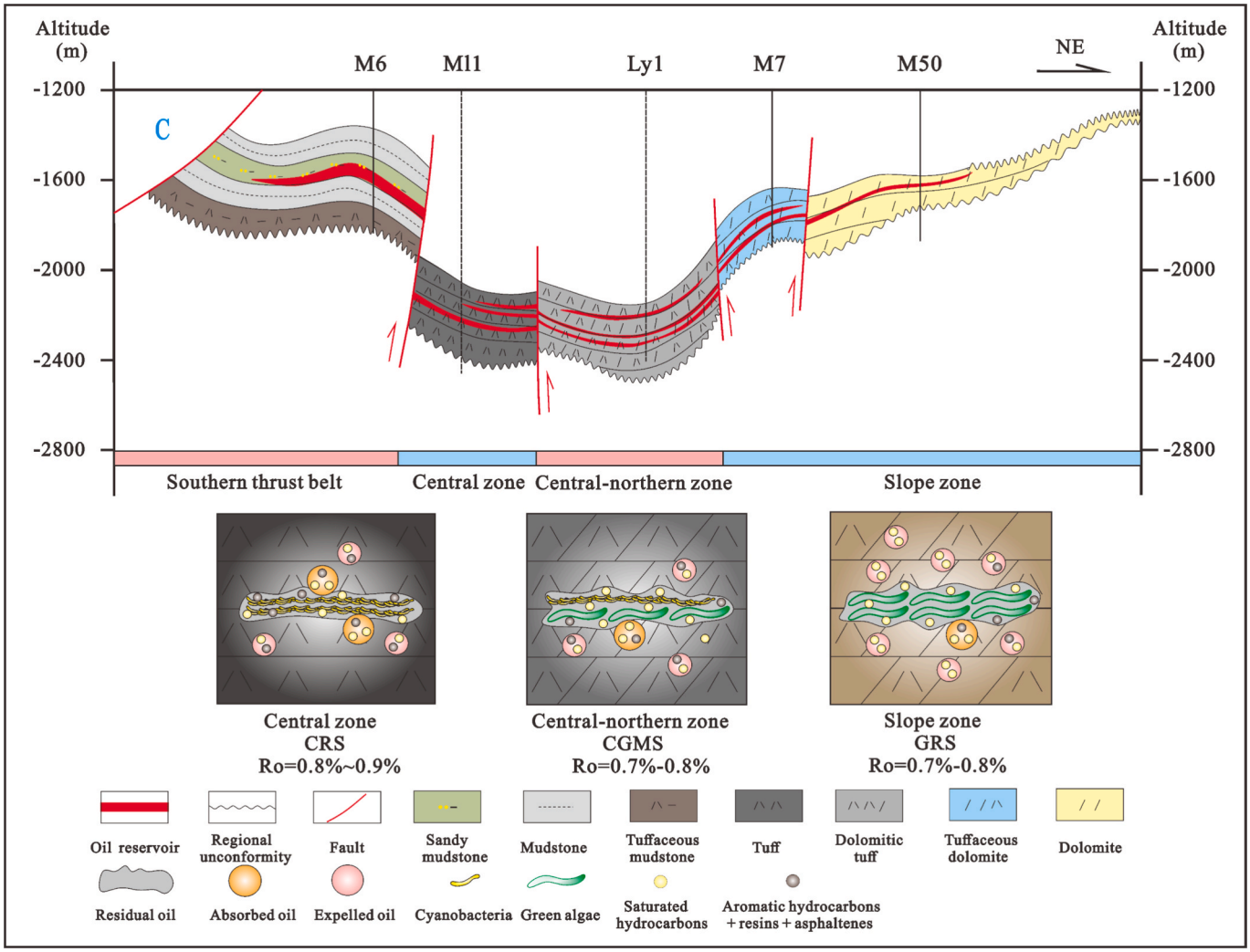

Fig. 9. Shale oil accumulation model of the P_2l^2 member in the Malang Sag, illustrating the distribution of CRS, GRS, and CGMS and their associated hydrocarbon enrichment characteristics; CRS: cyanobacteria-rich shale; GRS: green algae-rich shale; CGMS: cyanobacteria and green algae mixed shale. (For interpretation of the references to colour in this figure legend, the reader is referred to the web version of this article.)

increase in expelled oil yield during the late oil window, followed by gradual cracking (Fig. 8c3 and c4), with a gradual decrease in residual oil, and the properties of the generated hydrocarbons lie between those of the two end-member samples.

4.3. Implications

Previous studies suggest that different lithologies in the Malang Sag are distributed in a banded pattern [79]. The southern thrust belt primarily develops massive calcareous sandstones, the central zone consists mainly of pure tuff, the central-northern zone features transitional lithologies dominated by tuffaceous dolomite and dolomitic tuff, while the slope zone is primarily composed of tuffaceous dolomite and dolomite [79–81]. Based on the relationship between organic matter and lithology [37], the central zone mainly develops CRS, the central-northern zone primarily develops CGMS, and the slope zone mainly develops GRS (Fig. 9).

The P_2l^2 interval rocks are dense, with minimal micro-migration both between and within the layers, making the central zone, central-northern zone, and slope zone all source-reservoir integrated shale oil reservoirs [80,82,83]. The organic matter maturity in the central zone ranges from 0.79 % to 0.91 % (avg. 0.84 %), while in the central-northern and slope zones, it is lower, ranging from 0.70 % to 0.75 % (avg. 0.73 %) and 0.68 % to 0.74 % (avg. 0.71 %), respectively. Despite this, the M7 well area in the slope zone still exhibits high production, with the nearby M708 well producing 19.26 t of oil per day, and the cumulative oil production from the M1 well in the slope zone reaching ten thousand tons (Fig. 9). In contrast, the daily oil production from the LY1 and L1 wells in the central-northern zone is 0.21 t and 1.96 t, respectively, while the Ml1 well in the Central zone only produces 1.48 t of oil per day (Fig. 9). Additionally, the better crude oil properties in the slope zone compared to the central and central-northern zones indicate that oil production in different structural positions is closely related to the organic matter composition and thermal evolution [81]. Although the organic matter thermal evolution degree in the central and central-northern zones is higher than in the slope zone, the predominance of CRS in these zones leads to later hydrocarbon generation and poorer oil properties. In contrast, despite the lower organic matter maturity in the slope zone, GRS can generate better-quality oil at an earlier stage, resulting in a higher shale oil enrichment level, which makes it the main production area for the P_2l^2 interval shale oil at present [81].

In-situ conversion, which primarily involves heating to pyrolyze the originally immature organic matter and release more crude oil, is one of the key methods to improve shale oil mobility, especially given the generally low organic matter maturity in the P_2l^2 [3,84–87]. However, studies on different organic matter hydrocarbon generation and expulsion mechanisms show that in-situ conversion of CRS and CGMS from the central and central-northern zones generates more heavy residual oil (Fig. 8a2, a3, c2, and c3), making it difficult to release more movable oil in a short period. In contrast, as the organic matter maturity increases in GRS from the slope zone, a significant amount of light oil is quickly released (Fig. 8b1, b2, and b3), demonstrating greater potential for in-situ conversion. Therefore, the Slope zone is the preferred target for future engineering modifications.

Taking the Permian strata in northwest China as an example, multiple saline lake basins have developed, making them important targets for current oil and gas exploration [88,89]. Examples include the Fengcheng Formation in the Mahu Depression, the Lucaogou Formation in the Jimusaer Depression, the Pingdiquan Formation in the Shishugou Depression, and the Lucaogou Formation in the Jinan Depression, where recent breakthroughs have been made [12,13,90,91]. The organic matter in these shales has largely been confirmed to be dominated by Dunaliella (green algae), cyanobacteria, or Tasmanites [14,42], with these algae showing differential enrichment characteristics in response to changes in paleoclimate conditions [92–96]. This characteristic is highly similar with that of the P_2l^2 in the Santanghu Basin, providing a basis for comparison. Therefore, the findings from this study on hydrocarbon generation and expulsion mechanisms are also of reference value for the exploration and development of shale oil in similar saline lake basins.

5. Conclusions

This study systematically investigates the hydrocarbon generation, expulsion, and retention characteristics of CRS, GRS, and CGMS within the P_2l^2 member of the Malang Sag. By identifying the HEE and its controlling factors for each shale type, three conceptual models are proposed: (1) CRS—late oil generation and expulsion, narrow oil window, strong retention; (2) CGMS—early oil generation, late oil expulsion, wide oil window, moderate retention; and (3) GRS—early oil generation and expulsion, wide oil window, weak retention. These distinctions significantly influence shale oil enrichment across structural zones. In particular, the slope zone—dominated by GRS and capable of generating light hydrocarbons at an early stage—shows greater resource potential and represents a promising target for future in-situ conversion strategies.

Compared with previous pyrolysis studies, this work integrates hydrous pyrolysis with pre-/post-extraction pyrolysis to precisely quantify expelled, absorbed, and residual oil. Building on insights into differential organic matter enrichment, it enhances understanding of liquid hydrocarbon occurrence across different stages of thermal evolution. Given the global distribution of saline lacustrine shale systems, the findings offer practical insights into hydrocarbon generation and expulsion mechanisms applicable to a wide range of analogous depositional environments. However, lithological variability and heterogeneity in organic matter enrichment should be carefully considered when applying these conceptual models elsewhere.

CRediT authorship contribution statement

Miao Yu: Writing – original draft, Methodology, Investigation, Data curation, Conceptualization. **Gang Gao:** Writing – review & editing, Supervision, Methodology, Conceptualization. **Shengnan Chen:** Writing – review & editing, Supervision, Methodology, Conceptualization. **Jie Li:** Software, Investigation, Data curation. **Mingyu Liu:** Validation, Software, Data curation. **Jilun Kang:** Validation, Supervision, Project administration. **Xiongfei Xu:** Supervision, Project administration. **Wei Zhang:** Supervision, Investigation.

Declaration of competing interest

The authors declare that they have no known competing financial interests or personal relationships that could have appeared to influence the work reported in this paper.

Acknowledgments

We would like to acknowledge the financial support from PetroChina Tuha Oilfield Company (No. YJYHZC2022) and express our gratitude to the experts from the Exploration and Development Research Institute of Tuha Oilfield Company for their valuable assistance. Additionally, we extend our thanks to China University of Petroleum, Beijing, and the University of Calgary for providing advanced instruments and equipment, as well as professional guidance. We also sincerely thank the anonymous reviewers and the editor for their constructive comments and suggestions, which greatly improved the quality of this manuscript.

Appendix A. Supplementary data

Supplementary data to this article can be found online at https://doi.org/10.1016/j.fuel.2025.136296.

Data availability

Data will be made available on request.

References

[1] Laughrey CD, Lemmens H, Ruble TE, et al. Black shale diagenesis: insights from integrated high-definition analyses of post-mature Marcellus formation rocks, Northeastern Pennsylvania. PAPG Meeting 2009:5–10.
[2] Jarvie DM. Shale resource systems for oil and gas: Part 2: shale-oil resource systems. In: Breyer JA, editor. Shale Reservoirs: Giant Resources for the 21st Century. AAPG Memoir; 2012. p. 97–119.
[3] Zou C, Yang Z, Cui J, Zhu R, Hou L, Tao S, et al. Formation mechanism, geological characteristics and development strategy of nonmarine shale oil in China. Pet Explor Dev 2013;40:15–27.
[4] Scarlat N, Dallemand JF, Monforti-Ferrario F, et al. Renewable energy policy framework and bioenergy contribution in the European Union: an overview from National renewable energy action plans and progress reports. Renew Sustain Energy Rev 2015;51:969–85.
[5] Gao Z, Bai L, Hu Q, Yang Z, Jiang Z, Wang Z, et al. Shale oil migration across multiple scales: a review of characterization methods and different patterns. Earth Sci Rev 2024;254:104879.
[6] Curtis ME, Cardott BJ, Sondergeld CH, Rai CS. Development of organic porosity in the Woodford shale with increasing thermal maturity. Int J Coal Geol 2012;103.
[7] Hackley PC, Fishman N, Wu T, Baugher G. Organic petrology and geochemistry of mudrocks from the lacustrine Lucaogou Formation, Santanghu Basin, northwest China: application to lake basin evolution. Int J Coal Geol 2016;168:11–24.
[8] Burnham AK, Huss EB, Singleton MF. Pyrolysis kinetics for Green River oil shale from the saline zone. Fuel 1983;62:1199–204.
[9] Ruble TE, Lewan MD, Philp RP. New insights on the Green River petroleum system in the Uinta basin from hydrous pyrolysis experiments. AAPG Bull 2003;85:1333–71.
[10] Schmoker JW. A resource evaluation of the Bakken Formation (Upper Devonian and Lower Mississippian) continuous oil accumulation, Williston Basin. Mountain Geologist 1996;33:1–11.
[11] Soeder DJ. The successful development of gas and oil resources from shales in North America. J Petrol Sci Eng 2018;163:399–420.
[12] Zhi D, Tang Y, He W, Guo X, Zheng M, Huang L. Orderly coexistence and accumulation models of conventional and unconventional hydrocarbons in Lower Permian Fengcheng Formation, Mahu Sag, Junggar Basin. Pet Explor Dev Online 2021;48:1.
[13] Hou M, Qiu J, Zha M, Swennen R, Ding X, Ablimit I, et al. Significant contribution of haloalkaliphilic cyanobacteria to organic matter in an ancient alkaline lacustrine source rock: a case study from the Permian Fengcheng Formation, Junggar Basin, China. Mar Pet Geol 2022;128.
[14] Liu S, Misch D, Gang W, Li J, Jin J, Duan Y, et al. Evaluation of the tight oil "sweet spot" in the Middle Permian Lucaogou Formation (Jimusaer Sag, Junggar Basin, NW China): insights from organic petrology and geochemistry. Org Geochem 2023:177.
[15] Bechtel A, Jia J, Strobl SAI, Sachsenhofer RF, Liu Z, Gratzer R, et al. Paleoenvironmental conditions during deposition of the Upper Cretaceous oil shale sequences in the Songliao Basin (NE China): implications from geochemical analysis. Org Geochem 2012;46:76–95.
[16] Liang C, Cao Y, Jiang Z, Wu J, Guo S, Wang Y. Shale oil potential of lacustrine black shale in the Eocene Dongying depression: implications for geochemistry and reservoir characteristics. AAPG Bull 2017;101:11.
[17] Jarvie DM, Hill RJ, Ruble TE, Pollastro RM. Unconventional shale-gas systems: the Mississippian Barnett Shale of north-central Texas as one model for thermogenic shale-gas assessment. AAPG Bull 2007;91:475–99.
[18] Jarvie DM. Components and processes affecting producibility and commerciality of shale resource systems. Geol Acta 2014;12:307–25.
[19] Horsfield B, Disko U, Leistner F. The micro-scale simulation of maturation: outline of a new technique and its potential applications. Geol Rundsch 1989;78:361–73.
[20] Burnham AK, Sweeney JJ. A chemical kinetic model of vitrinite maturation and reflectance. Geochim Cosmochim Acta 1989;53:2649–57.
[21] Souza IVAF, Araujo CV, Menezes TR, Coutinho LFC, Binotto R, Spigolon ALD, et al. Organic and mineral matter changes due to oil generation, saturation and expulsion process based on artificial maturation experiments. Geol Acta 2014;12:351–62.
[22] Stockhausen M, Galimberti R, Elias R, Di Paolo L, Schwark L. The Expulsinator versus conventional pyrolysis: the differences of oil/gas generation and expulsion simulation under near-natural conditions. Mar Pet Geol 2020;117:104412.
[23] Shi KY, Chen JQ, Pang XQ, et al. Average molecular structure model of shale kerogen: experimental characterization, structural reconstruction, and pyrolysis analysis. Fuel 2024;355:129474.
[24] Pepper AS, Corvi PJ. Simple kinetic models of petroleum formation. Part I: oil and gas generation from kerogen. Mar Pet Geol 1995;12:291–319.
[25] Eseme E, Littke R, Krooss BM, Schwarzbauer J. Experimental investigation of the compositional variation of petroleum during primary migration. Org Geochem 2007;38:1373–97.
[26] Yu M, Gao G, Jin J, Liu S, Zhang Y, Li WB. Hydrocarbon generation simulation and source rock studies in the Lower Assemblage, southern Junggar Basin, based on data from Gaotan 1 well. Pet Exp Geol 2022;44:687–97.
[27] Liao L, Wang Y, Chen C, Pan Y. Application of the grain-based rock-eval pyrolysis method to evaluate hydrocarbon generation, expulsion, and retention of lacustrine shale. Front Earth Sci 2022;10:921806.
[28] Sun Y, Wang Y, Liao L, Shi S, Liu J. How grain size influences hydrocarbon generation and expulsion of shale based on Rock-Eval pyrolysis and kinetics. Mar Pet Geol 2023;177:104956.
[29] Peters KE, Moldowan JM, Sundararama P. Effects of hydrous pyrolysis on biomarker thermal maturity parameters: Monterey Phosphatic and Siliceous members. Org Geochem 1990;15:249–65.
[30] Lewan MD. Laboratory simulation of petroleum formation: Hydrous pyrolysis. In: Engel M, Macko S, editors. Organic Geochemistry. New York: Plenum Publications Corp; 1993. p. 419–42.
[31] Lewan MD. Evaluation of petroleum generation by hydrous pyrolysis experimentation. Philos Trans R Soc Lond A 1985;315:123–34.
[32] Behar F, Vandenbroucke M, Tang Y, Marquis F, Espitalie J. Thermal cracking of kerogen in open and closed systems: determination of kinetic parameters and stoichiometric coefficients for oil and gas generation. Org Geochem 1997;26:321–39.
[33] Schenk HJ, Horsfield B. Using natural maturation series to evaluate the utility of parallel reaction kinetics models: an investigation of Toarcian shales and Carboniferous coals, Germany. Org Geochem 1998;29:137–54.
[34] Lewan MD, Roy S. Role of water in hydrocarbon generation from Type-I kerogen in Mahogany oil shale of the Green River Formation. Org Geochem 2011;42:31–41.
[35] Liu B, Song Y, Zhu K, Su P, Ye X, Zhao W. Mineralogy and element geochemistry of salinized lacustrine organic-rich shale in the Middle Permian Santanghu Basin: implications for paleoenvironment, provenance, tectonic setting and shale oil potential. Mar Pet Geol 2020;120.
[36] Pan Y, Huang Z, Li T. Environmental response to volcanic activity and its effect on organic matter enrichment in the Permian Lucaogou Formation of the Malang Sag, Santanghu Basin, northwest China. Palaeogeogr Palaeoclimatol Palaeoecol 2020;560:110024.
[37] Yu M, Gao G, Liu M, Liang H, Zhou Y, Zhao Z, et al. Sedimentary environment shift and organic matter enrichment mechanism in response to volcanic ash influence: a case study of the Permian Lucaogou Formation, Santanghu Basin, NW China. J Palaeogeogr 2024;13:792–809.
[38] Pan Y, Huang Z, Guo X, Li T, Zhao J, Li Z, et al. Lithofacies types, reservoir characteristics, and hydrocarbon potential of the lacustrine organic-rich fine-grained rocks affected by tephra of the Permian Lucaogou Formation, Santanghu Basin, western China. J Petrol Sci Eng 2022;208:109230.
[39] Sandvik EI, Young WA, Curry DJ. Expulsion from hydrocarbon sources: the role of organic absorption. Org Geochem 1992;19:77–87.
[40] Castañeda IS, Schouten S. A review of molecular organic proxies for examining modern and ancient lacustrine environments. Quat Sci Rev 2011;30:2851–91.
[41] Mishra CS, Samanta U, Gupta A, Thomas NJ, Misra KN. Hydrous pyrolysis of a Type III source: fractionation effects during primary migration in natural and artificially matured samples. Org Geochem 1996;25:489–505.
[42] Feng D, Liu C, Yang H, Han Y, Li G, Awan RS, et al. Experimental investigation of hydrocarbon generation, retention, and expulsion of saline lacustrine shale: Insights from improved semi-open pyrolysis experiments of Lucaogou Shale, eastern Junggar Basin, China. J Anal Appl Pyrolysis 2024;181:106640.
[43] Yu M, Gao G, Liang H, Jin J, Zhu K, Liu K, et al. Differential hydrocarbon generation characteristics of organic matter with green algae and cyanobacteria origins in the Permian Lucaogou Formation of the Santanghu Basin. J Anal Appl Pyrolysis 2024;168:105934.
[44] Tengger T, Tao C, Hu G, Shen BJ, Ma ZL, Pan AY, et al. The effect of expulsion efficiency on the formation and enrichment of shale gas. J Pet Exp Geol 2020;42(3).
[45] Ma W, Luo X, Tao S, Liu J, Guan P. Modified pyrolysis experiments and indexes to re-evaluate petroleum HEE and productive potential of the Chang 7 shale, Ordos Basin, China. J Petrol Sci Eng 2020;186:106710.
[46] Lafargue E, Espitalie J, Eggen S. Experimental simulation of hydrocarbon expulsion. Org Geochem 1990;16:121–31.
[47] Pang X, Li S, Jin Z, et al. Quantitative assessment of hydrocarbon expulsion of petroleum systems in the Niuzhuang Sag, Bohai Bay Basin, East China. Acta Geol Sin (Engl Ed) 2004;78:615–25.
[48] Dickey PA. Possible primary migration of oil from source rock in oil phase: geologic notes. AAPG Bull 1975;59:337–45.
[49] Leythaeuser D, Schaefer RG, Yukler A, et al. Role of diffusion in primary hydrocarbons. AAPG Bull 1982;66:408–29.
[50] Hou L, Luo X, Han W, Lin S, Pang Z, Liu J. Geochemical evaluation of the hydrocarbon potential of shale oil and its correlation with different minerals: a case study of the TYP shale in the Songliao Basin, China. Energy Fuel 2020;34:11998–2009.
[51] Connan J. Biodegradation of crude oils in reservoirs. In: Brooks J, Welte DH, editors. Advances in petroleum geochemistry. London: Academic Press; 1984. p. 299–335.
[52] Li J, Ma W, Wang YF, Wang DL, Xie ZY, Li ZS, et al. Simulated pyrolysis experiment of sapropelic source rocks and the full process hydrocarbon evolution model. Pet Explor Dev 2018;45(3):445–54.
[53] Zhao WZ, Hu SY, Hou LH, Yang T, Li X, Guo BC, et al. Types, resource potential, and boundaries between lacustrine shale oil and tight oil in China. Pet Explor Dev 2020;47(1):1–10.
[54] Zhang W, Yang H, Li J, Zhang Y, Zhang L, Zhi Z, et al. Leading effect of high-class source rock of Chang 7 in Ordos Basin on enrichment of low permeability oil-gas accumulation: hydrocarbon generation and expulsion mechanism. Pet Explor Dev 2006;33:289–93.

[55] Gao G, Liu SJ, Jin J, et al. A new discovery of physical property evolution of crude oil and insights into shale oil exploration. Acta Geol Sin 2023;97(5):703–17.
[56] Yu M, Gao G, Ma WY, Jin J, Liu S, Zhang Y, et al. Hydrocarbon generation differences of shales composed of green algae and cyanobacteria: a case study of Mesozoic and Cenozoic saline lacustrine shales in the Junggar Basin, NW China. Pet Sci 2023;20:3348–62.
[57] Liu B, Meng QA, Fu XF, et al. Composition of generated and expelled hydrocarbons and phase evolution of shale oil in the 1st member of Qingshankou Formation, Songliao Basin. Pet Nat Gas Geol 2024;45(2):406–19.
[58] Zou CN, Zhang GS, Yang Z, et al. Unconventional oil and gas concepts, characteristics, potential, and technologies: a review of unconventional oil and gas geology. Pet Explor Dev 2013;40(4). 385–399+454.
[59] Abrams MA, Gong C, Garnier C, Sephton MA. A new thermal extraction protocol to evaluate liquid rich unconventional oil in place and in-situ fluid chemistry. Mar Pet Geol 2017;88:659–75.
[60] Zeng F, Dong C, Lin C, Wu Y, Tian S, Zhang X, et al. Analyzing the effects of multi-scale pore systems on reservoir properties: a case study on Xihu depression, East China Sea Shelf Basin,China. J Petrol Sci Eng 2021;203:108609.
[61] Feng D, Liu C, Yang X, Su J, Yang H, Han Y. Pyrolysis product characteristics and hydrocarbon generation–retention–expulsion model of alkaline lacustrine organic-rich shale. Fuel 2025;395:135239.
[62] Halbouty MT. Giant Oil and Gas Fields of the 1990s: An Introduction. Tulsa: AAPG Memoir; 2003. p. 78.
[63] Liu B, Bechtel A, Sachsenhofer RF, Gross D, Gratzer R, Chen X. Depositional environment of oil shale within the second member of Permian Lucaogou Formation in the Santanghu Basin, Northwest China. Int J Coal Geol 2017;175.
[64] Lu F, Tan X, Xiao D, Shi K, Li M, Zhang Y, et al. Sedimentary control on diagenetic paths of dolomite reservoirs in a volcanic setting: a case study of the Permian Chihsia Formation in the Sichuan Basin, China. Sediment Geol 2023;454:106964.
[65] Yu M, Gao G, Zhao X, Liu Y, Luo Q. Sedimentary environment and a development model for source rocks rich in the green alga Pediastrum: a case study of the Paleogene Anjihaihe Formation in the Junggar Basin, Northwest China. Int J Earth Sci 2024;113:1883–902.
[66] Shi KY, Chen JQ, Pang XQ, et al. Wettability of different clay mineral surfaces in shale: implications from molecular dynamics simulations. Petroleum Science 2023; 20(2):689–704.
[67] He J, Lian Z, Luo W, Zhou H, Xu H, He P, et al. Characteristics and main controlling factors of intra-platform shoal thin-layer dolomite reservoirs: a case study of Middle Permian Qixia Formation in Gaoshiti-Moxi area of Sichuan Basin, SW China. Pet Explor Dev 2024;51:69–80.
[68] Guo X, Zhou L, Pan Y, Huang Z, Chen X, Mu S, et al. Pore structure and oil-bearing property of laminated and massive shale of Lucaogou Formation in Malang Sag. Santanghu Basin. Geol J 2023;59:980–99.
[69] Akkutlu IY, Baek S, Olorode OM, Wei P, Tongyi Z, Shuang A. In: Shale Resource Assessment in Presence of Nanopore Confinement, Unconventional Resources Technology Conference, Austin, Texas, 24-26 July 2017, p. 1431–51.
[70] Saberi F, Hosseini-Barzi M. Effect of thermal maturation and organic matter content on oil shale fracturing. Int J Coal Sci Technol 2024;11:53–66.
[71] Braun RL, Burnham AK. Mathematical model of oil generation, degradation and expulsion. Energy Fuels 1990;4:132–46.
[72] Saif T, Lin Q, Singh K, Bijeljic B, Blunt MJ. Dynamic imaging of oil shale pyrolysis using synchrotron X-ray microtomography. Geophys Res Lett 2016;43:6799–807.
[73] Saif T, Lin Q, Gao Y, Al-Khulaifi Y, Marone F, Hollis D, et al. 4D in situ synchrotron X-ray tomographic microscopy and laser-based heating study of oil shale pyrolysis. Appl Energy 2019;235:1468–75.
[74] Kim TW, Ross CM, Guan KM, Burnham AK, Kovscek AR. Permeability and porosity evolution of organic-rich shales from the Green River formation as a result of maturation. SPE J 2020;25:1377–405.
[75] Turakhanov A, Tsyshkova A, Mukhina E, Popov E, Kalacheva D, Dvoretskaya E, et al. Cyclic subcritical water injection into Bazhenov oil shale: geochemical and petrophysical properties evolution due to hydrothermal exposure. Energies 2021; 14:4570.
[76] Kelemen SR, Siskin M, Gorbaty ML, Kwiatek PJ, Niskodé W, Strauss BG, et al. Petroleum expulsion Part 3. A model of chemically driven fractionation during expulsion of petroleum from kerogen. Energy Fuels 2006;20:309–19.
[77] Thomas MM, Clouse JA. Primary migration by diffusion through kerogen: I. Model experiments with organic-coated rocks. Geochim Cosmochim Acta 1990;54: 2775–9.
[78] Thomas MM, Clouse JA. Primary migration by diffusion through kerogen: II. Hydrocarbon diffusivities in kerogen. Geochim Cosmochim Acta 1990;54:2781–92.
[79] Xu XF, Yu XC, Qing Z, et al. Lithofacies characteristics and their relationship with shale oil reservoirs in the Luocaogou Member of the Santanghu Basin. Xinjiang Pet Geol 2020;41(6):677–84.
[80] Liu B, Lv YF, Zhao R, et al. The overpressure and shale oil enrichment mechanisms of the mud shale system in the Luocaogou Member in the Malang Sag of the Santanghu Basin. Pet Explor Dev 2012;39(6):699–705.
[81] Fan T, Xu X, Fan L, et al. Geological characteristics and exploration prospect of shale oil in Permian Lucaogou Formation, Santanghu Basin. China Pet Explor 2021; 26:125–36.
[82] Liu B, Lv YF, Meng YL, et al. Characteristics, genetic models, and shale oil implications of lake facies laminated fine-grained rocks: a case study from the Permian Luocaogou Member in the Malang Sag, Santanghu Basin. Pet Explor Dev 2015;42(5):598–607.
[83] Fang X, Yang Z, Wu Y. Analysis of the main controlling factors for the enrichment of tight oil in the Luocaogou Member of the Santanghu Basin. Geol Rev 2021;67 (S1):217–8.
[84] Kang Z, Zhao Y, Yang D. Review of oil shale in-situ conversion technology. Appl Energy 2020;269:115024.
[85] Hou H, Du Q, Huang C, Zhang L, Hu E. An oil shale recovery system powered by solar thermal energy. Energy 2021;225.
[86] Han W, Luo X, Tao S, Lin S, Liu J, Yang Y. Activation energy and organic matter structure characteristics of shale kerogen and their significance for the in-situ conversion process of shale oil. Fuel 2024;370:127622.
[87] Hu X, Lu Y, Li W, Wang L, Huang X, Yang D. The effects of crustal stress and supercritical water pressure on the in-situ pyrolysis characteristics of Balikun oil shale. J Energy Inst 2024;103:162–76.
[88] Liu G, Wang G, Li N, He H, Lu N, Lei Q, et al. Characteristics and geological significance of carbon and oxygen isotopes of the Permian Lucaogou Formation dolomite in the southern Junggar Basin, northwestern China. J Palaeogeogr 2024; 13:862–82.
[89] Zeng W, Wang B, Chen X, Fu G, Zhang Z, Huang Z. Geochemical characteristics and formation mechanism of organic-rich source rocks of mixed sedimentary strata in continental saline lacustrine basin: a case study of Permian Pingdiquan Formation in the Shishugou Sag, Junggar Basin, Northwest China. Int J Coal Geol 2024;287: 104900.
[90] Liang SJ, Luo QS, Kang JL, Li FL, Ma Q, Wang XC, et al. Risk exploration breakthrough and significance of well Sta1 in the Jinnan Sag, Junggar Basin. China Petroleum Exploration 2021;26(4):72–83.
[91] Zhang W, Zhao LL, Gong X, Wang XC, Wang YJ. Geochemical characteristics of hydrocarbon source rocks of the Pingdianquan Formation in the Shishugou Sag, Junggar Basin. Pet Geol Eng 2022;36(3):27–32.
[92] Xia LW, Cao J, Xu TW, Wang TT, Zhang YX, Bian LZ, et al. Characteristics of biological development in saline lakes and their source rock implications. Geol Rev 2017;63(6):1549–62.
[93] Dang W, Gao G, You X, Wu J, Liu S, Yan Q, et al. Genesis and distribution of oils in Mahu Sag, Junggar Basin, NW China. Pet Explor Dev Online 2023;50:4.
[94] Cao Y, Jin Z, Zhu R, Liu K, Bai J. Comprehensive evaluation of the organic-rich saline lacustrine shale in the Lucaogou Formation, Jimusar Sag, Junggar Basin, NW China. Energy 2024;294:120603.
[95] Man L, Duan G, Zhang T, Liu N, Song Y, Zhang Z, et al. Influences of paleoclimatic changes on organic matter enrichment mechanisms in freshwater and saline lacustrine oil shale in China: a machine learning approach. Earth Sci Rev 2025;262: 104056.
[96] Zeng W, Zhang Z, Wang B, Chen X, Zheng R, Fu G, et al. Formation mechanism of organic-rich mixed sedimentary rocks in saline lacustrine basin, Permian Lucaogou Formation, Jimsar Sag, Junggar Basin, Northwest China. Mar Pet Geol 2023;156: 104362.